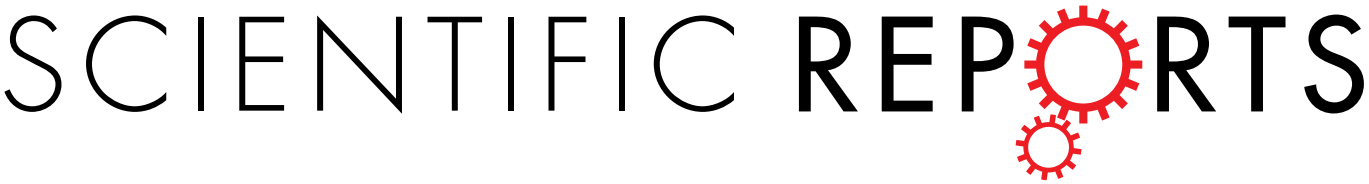

OPEN

Received: 2 August 2017
Accepted: 16 October 2017
Published online: 02 November 2017

Turbulent transport reduction induced by transition on radial electric field shear and curvature through amplitude and cross-phase in torus plasma

T. Kobayashi[1], K. Itoh[1,2,3], T. Ido[1], K. Kamiya[4], S.-I. Itoh[3,5], Y. Miura[6], Y. Nagashima[3,5], A. Fujisawa[3,5], S. Inagaki[3,5] & K. Ida[1,3]

Spatiotemporal evolutions of radial electric field and turbulence are measured simultaneously in the H-mode transition, which is a prototypical example of turbulence structure formation in high-temperature plasmas. In the dynamical phase where transport barrier is established abruptly, the time-space-frequency-resolved turbulent particle flux is obtained. Here we report the validation of the mechanism of transport barrier formation quantitatively. It is found that the particle flux is suppressed predominantly by reducing density fluctuation amplitude and cross phase between density fluctuation and potential fluctuation. Both radial electric field shear and curvature are responsible for the amplitude suppression as was predicted by theory. Turbulence amplitude reduction immediately responds to the growth of the radial electric field non-uniformity and saturates, while cross phase continuously approaches zero.

Structure of flows and turbulence in non-equilibrium plasmas has attracted much attention because of its great impact on the entire media dynamics. One of the prototypical examples can be seen in the solar tachocline[1], across which the transition from the differential rotation in the solar convective zone to the rigid rotation in the radiative interior occurs. The strong shear flow within the thin layer is believed to amplify the magnetic field as the solar dynamo. Another example is the edge transport barrier (ETB) in toroidal fusion plasmas[2], which is spontaneously formed in the Low-confinement mode to High-confinement mode transition (L-H transition)[3]. Because of its rich nature of nonlinear dynamics as well as its promising capability for achieving good plasma performance toward the fusion reactor, much attention has been paid for clarifying the underlying physics for decades. Numerous studies have shown essential roles of an edge-localized poloidal $E \times B$ flow structure on confinement improvement[4–7]. However, definitive conclusion regarding what aspect of the $E \times B$ flow suppresses the turbulent transport is still under debate[8]. In order to obtain an understanding based on first principles, interplay between the flow structure and the turbulence must be diagnosed with high spatiotemporal resolutions, which remains challenging.

In modeling works, roles of inhomogeneous $E \times B$ flow on the turbulence suppression are classified in two elements: shear and curvature. Effects of both non-uniformities on mode instability were discussed[9,10]. Nonlinear saturation level of turbulence was studied using a statistical approach, showing an essential role of both shear and curvature of the $E \times B$ flow[11]. In a newly developed model[12] described in "Method", shear and curvature were simultaneously treated in a single formulae that provided turbulence reduction rate. In that model, responsible physics of shear and curvature were considered as the $E \times B$ flow shear decorrelation of turbulence eddy[13–15] and

[1]National Institute for Fusion Science, National Institutes of Natural Sciences, Toki, 509-5292, Japan. [2]Institute of Science and Technology Research, Chubu University, Kasugai, 487-8501, Japan. [3]Research Center for Plasma Turbulence, Kyushu University, Kasuga, 816-8580, Japan. [4]National Institute for Quantum and Radiological Science and Technology, Naka, 311-0193, Japan. [5]Research Institute for Applied Mechanics, Kyushu University, Kasuga, 816-8580, Japan. [6]Japan Atomic Energy Agency, Tokai, 319-1184, Japan. Correspondence and requests for materials should be addressed to T.K. (email: kobayashi.tatsuya@LHD.nifs.ac.jp)

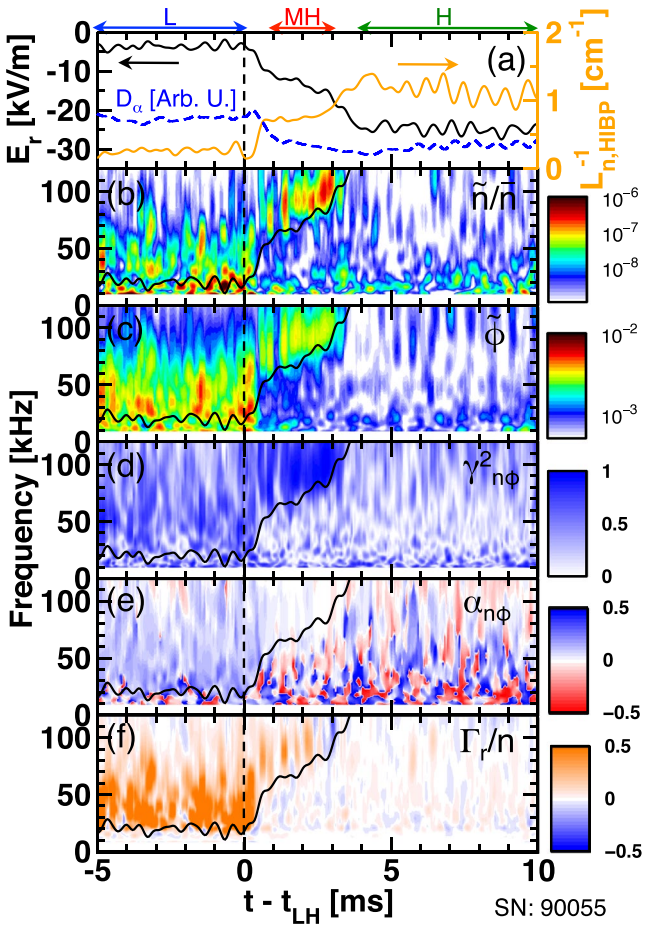

Figure 1. Time traces of (**a**) D_α emission, inverse density gradient length and radial electric field, wavelet power spectra of (**b**) relative density fluctuation and (**c**) potential fluctuation, (**d**) and (**e**) squared cross coherence and cross phase between density fluctuation and potential fluctuation, respectively, and (**f**) particle flux normalized by mean density at $r - a \sim -0.8$ cm. Black curves on contour plots show the expected frequency Doppler shift in the laboratory frame.

the modulational coupling causing energy transfer from turbulence to macroscopic $E \times B$ flow structure[2,12,16], respectively. Experimental examinations of those models have been performed[8,17–25]. Focusing on detailed physics of transport suppression, direct fluctuation measurement by use of electrostatic probes has been promoted. It was found that the turbulent particle flux is reduced not only by the density fluctuation amplitude suppression but also by the cross phase alternation between the density fluctuation and the potential fluctuation[19–22]. Although individual elements regarding the turbulent transport suppression by the inhomogeneous $E \times B$ flow have been raised, i.e., shear and curvature of $E \times B$ flow and amplitude and cross phase of fluctuations, the mutual relation of these elements remain unclear.

In this paper, we investigate response of turbulent particle flux on radial electric field non-uniformity by analyzing data from a heavy ion beam probe (HIBP). In particular, interrelations among shear and curvature of radial electric field and amplitude and cross phase of fluctuations are shown for the first time. Electron density and electrostatic potential measured with high spatiotemporal resolutions allow us to perform time-space-frequency-decomposition to the fluctuation induced particle flux. The particle flux is suppressed predominantly by reducing both the density fluctuation amplitude and the cross phase between density fluctuation and potential fluctuation. Both curvature and shear are responsible for transport reduction. Turbulence amplitude reduction immediately responds to the growth of the radial electric field non-uniformity and saturates, while cross phase continuously approaches zero. The time scales of these dynamics have an order of magnitude difference. As a result, turbulent transport reduction occurs with two different time scales.

Results

Time-space-frequency-resolved turbulence spectrum. Figure 1 (a) shows time evolutions of D_α emission from divertor region, inverse density gradient length $L^{-1}_{n,\mathrm{HIBP}} \equiv -\nabla I_{\mathrm{HIBP}}/I_{\mathrm{HIBP}}$, where I_{HIBP} is the HIBP secondary beam current that reflects the local electron density, and radial electric field E_r at $r - a \sim -0.8$ cm, in which the bottom of the E_r-well structure emerges in H-mode. The global profile changes are represented by low-pass filtered signals with a cut-off frequency of 2 kHz. The cut-off frequency is chosen to eliminate dynamics of

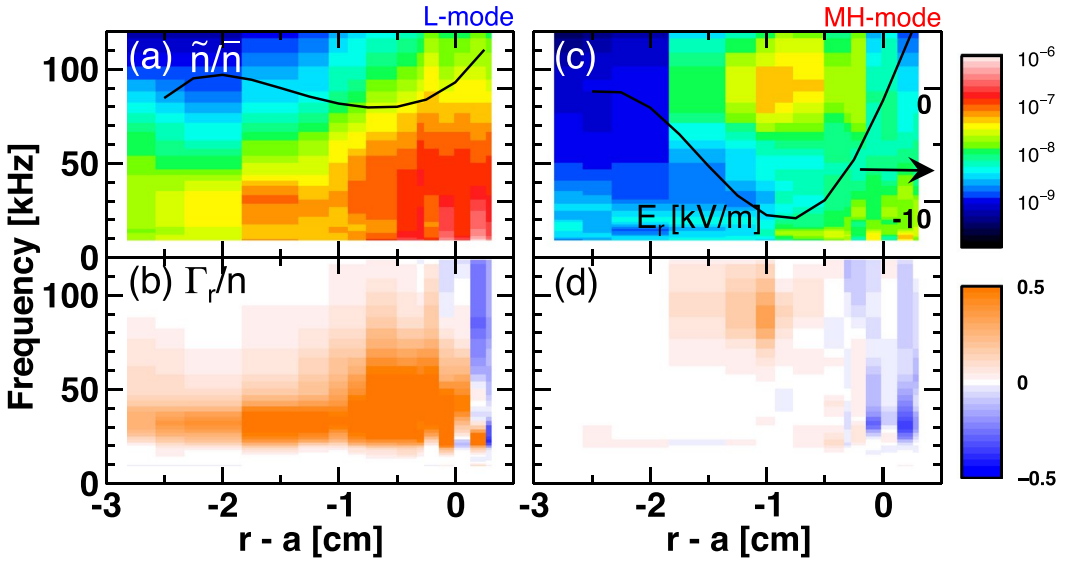

Figure 2. Radial profiles of time averaged wavelet spectra of (**a** and **c**) relative density fluctuation and (**b** and **d**) particle flux normalized by mean density in L-mode and in MH-mode, respectively. Black curves in (**a**) and (**c**) are radial profile of radial electric field.

the limit-cycle oscillation at 4.5 kHz[26]. As clearly indicated, transition in $L_{n,\mathrm{HIBP}}^{-1}$ and E_r occurs twice[27]. The first transition is triggered by the reach of a sawtooth crash-induced heat pulse at the edge region. The onset time t_{LH} is defined using the D_α emission signal and a soft-x-ray signal. After the first transition within several hundred microseconds, the plasma experiences a short period quasi-stationary state of ~2 ms, which we call the "MH-mode" (meta-stable H-mode). Then, the plasma reaches the final H-mode by completing the transport barrier with the second transition within ~1 ms. A dedicated study revealed that the radial current induced by the neoclassical bulk viscosity[4,5], and the ion loss-cone loss[5] plays an important role for building E_r structure during the first transition[28]. Reynolds stress driven E_r was found to be much smaller.

Contour plots in Fig. 1 show time-frequency-resolved wavelet power spectra of (b) relative density fluctuation $\tilde{n}/\bar{n}$ and of (c) potential fluctuation $\tilde{\phi}$, (d) and (e) squared cross coherence and cross phase between $\tilde{n}$ and $\tilde{\phi}$ denoted as $\gamma_{n\phi}^2$ and $\alpha_{n\phi}$, respectively, and (f) particle flux normalized by mean density Γ_r/n. Here, wavelet transform is performed with a time interval of 50 μs, after which four sequential time samples are ensemble averaged. Squared cross coherence and cross phase are defined as $\gamma_{n\phi}^2 = |P_{n,\phi}|^2/P_nP_\phi$ and $\alpha_{n\phi} = tan^{-1}\mathrm{Re}[P_{n,\phi}]/\mathrm{Im}[P_{n,\phi}]$ with the power spectrum of $\tilde{n}$ and $\tilde{\phi}$ and cross spectrum between them denoted as P_n, P_ϕ, and $P_{n,\phi}$, respectively. The particle flux is defined as $\Gamma_r = B^{-1}(P_nP_\phi\gamma_{n\phi}^2)^{1/2}k_\theta \sin\alpha_{n\phi}$[29]. The poloidal wavenumber of turbulence k_θ is determined to be $k_\theta \sim 0.75\ \mathrm{cm}^{-1}$ in $f > 20$ kHz in a dedicated discharge, in which the sample volumes of HIBP are aligned in a magnetic surface at $r - a \sim -1$ cm[30]. The poloidal wavenumber in $f < 20$ kHz is much smaller compared to that in $f > 20$ kHz so that the particle flux driven by those low frequency components play a minor role for confinement. In this paper, the poloidal direction is defined as the electron diamagnetic direction. At the central frequency $f \sim 50$ kHz, phase velocity is approximately equal to the electron diamagnetic velocity in the plasma frame.

Properties of turbulence and turbulent particle flux change drastically through the transitions. In L-mode, a broadband turbulence spectrum in $f < 80$ kHz arises both in $\tilde{n}/\bar{n}$ and $\tilde{\phi}$ spectra. Cross phase $\alpha_{n\phi}$ is slightly positive in average and turbulence-driven particle flux is directed outward. During the L-MH transition, the central frequency of the turbulence spectrum rises sharply up to ~100 kHz. Black curves superimposed on Fig. 1 (b)-(f) show the expected Doppler frequency shift for turbulence component at $f = 20$ kHz in L-mode, where k_θ is assumed to remain unchanged through L-MH transition. Below the curve, amplitude of fluctuation is significantly reduced, in which fluctuation wavenumber is found to be substantially lower than that of the high frequency turbulence component[30]. In contrast, the higher frequency component suffers a moderate amplitude reduction. Squared cross coherence $\gamma_{n\phi}^2$ remains close to unity but cross phase $\alpha_{n\phi}$ decreases toward zero. A considerable reduction of the particle flux occurs, which is responsible for density pedestal formation. Further deepening of the E_r-well occurs in the final H-mode. Doppler shifted frequency exceeds measurable frequency band. Therefore we avoid investigating the final H-mode period in this paper.

Figure 2 shows radial profile of time-averaged turbulence spectrum. Radial profile of E_r is superimposed as black curves. In L-mode, turbulence has a broad spectrum both in frequency and in space. This broadband turbulence generates a widely distributed outward directed particle flux that is related to the confinement degradation. After the L-MH transition, the E_r-well structure with the full width at half maximum of ~1.4 cm emerges at $r - a = -0.8$ cm. In MH-mode, Doppler frequency shift occurs up to ~100 kHz with a moderate amplitude reduction at the bottom of the E_r-well. The Doppler frequency shift is only visible within the E_r-well. While, the turbulence is strongly stabilized in the outer shear region ($r - a > -0.3$ cm), the inner shear region

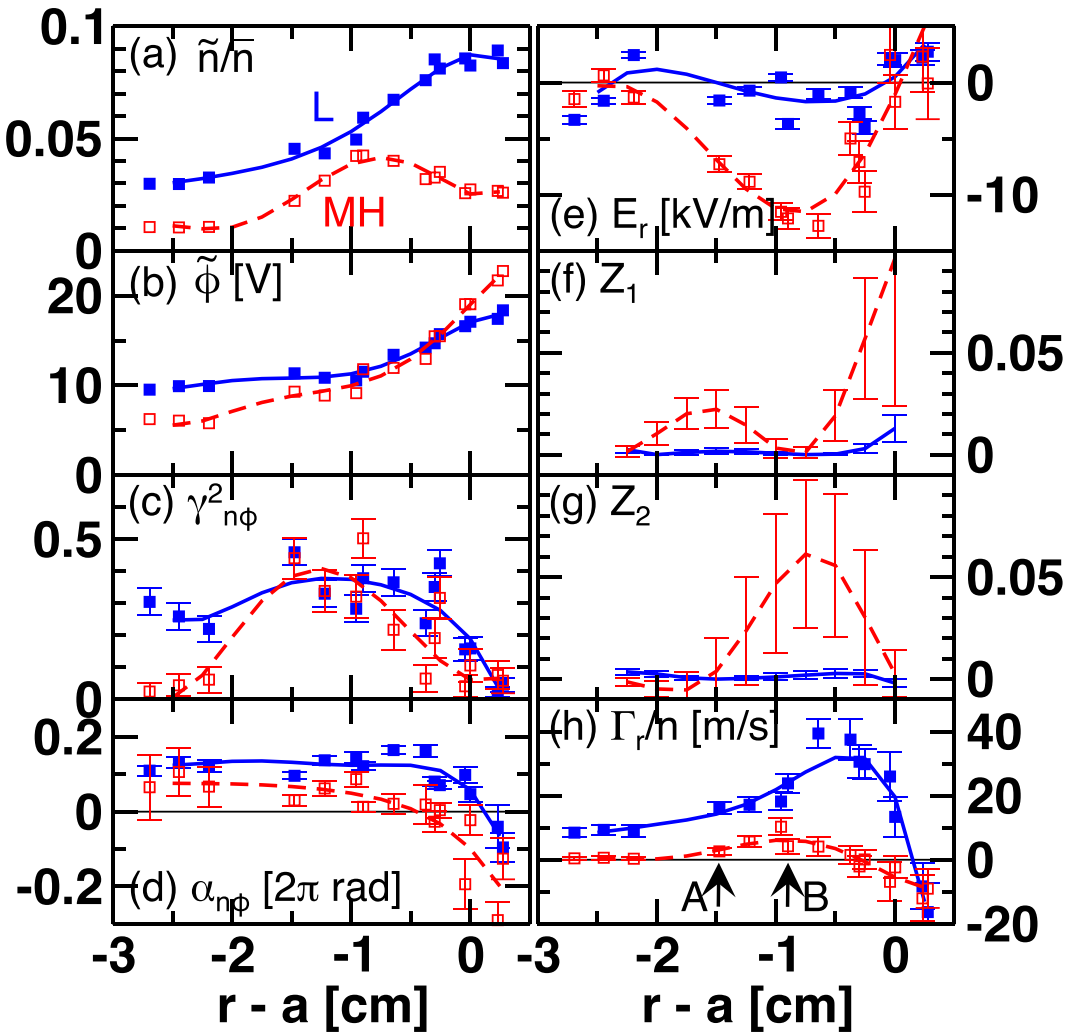

Figure 3. Radial profiles of (**a**) relative density fluctuation amplitude, (**b**) potential fluctuation amplitude, (**c**) and (**d**) squared cross coherence and cross phase between density fluctuation and potential fluctuation, respectively, (**e**) radial electric field, (**f**) shear parameter Z_1, (**g**) curvature parameter Z_2, and (**h**) particle flux normalized by mean density. Arrows labeled "A" and "B" in (**h**) indicate radii in which detailed time traces are shown in Fig. 4.

(−1.8 cm $< r - a <$ −1.3 cm), and further inside ($r - a <$ −1.8 cm). As a result, the outward particle flux is entirely suppressed outside the E_r-well. Even inside the E_r-well, the particle flux is clearly reduced mainly because of change in the cross phase $\alpha_{n\varphi}$ as discussed above.

Response of turbulent particle flux on radial electric field non-uniformity. On frequency integrated turbulence properties shown in Fig. 3, we quantitatively show response of turbulent particle flux on radial electric field non-uniformity. Radial profiles of fluctuation amplitude for $\tilde{n}/\bar{n}$ and $\tilde{\phi}$ [Fig. 3(a) and (b)] are given by integrating the spectra in 20 kHz $\leq f \leq$ 110 kHz. In L-mode, shapes of both amplitude profiles are similar and normalized turbulence amplitudes are approximately in the same level, $e\tilde{\phi}/T_e \sim \tilde{n}/\bar{n}$, where an equivalent order of electron temperature and ion temperature $T_e \sim T_i$ is assumed[7], and $T_i \sim 130$ eV is obtained by a charge exchange spectroscopy. A small but finite phase difference between density fluctuation and potential fluctuation exists. The dominant turbulence source is considered as the resistive drift wave[26]. Two different elements of radial electric field non-uniformity, shear and curvature, are parameterized as non-dimensional factors Z_1 and Z_2, respectively. See "Method" for the definition. Radial profiles of Z_1 and Z_2 are shown in Fig. 3(f) and (g). Spatial derivative is taken for fifth order polynomial fit of the E_r profile. The model[12] predicts that the non-uniformity observed here is large enough to suppress turbulence amplitude, i.e., $(k\rho_i)^{-2}(Z_1 + Z_2) > 1$, where the turbulence scale factor is given as $(k\rho_i)^{-2} \sim 0.01$. Note that the criterion for Z_1 is equivalent to the well-known shearing rate criterion[13], i.e., $\partial|E_r/B|/\partial r > \gamma_L$, if the turbulence decorrelation rate γ_L can be approximated by the drift wave frequency kV_d. The criterion for Z_2 corresponds to $\sqrt{|E_r E_r''/B^2|} > kV_d$[16]. At the location where $(k\rho_i)^{-2}Z_2 > 1$ is held, a substantial fraction of the microscopic turbulence energy is transferred into the macroscopic radial electric field. If the transferred energy is large enough to maintain the radial electric field structure, the H-mode

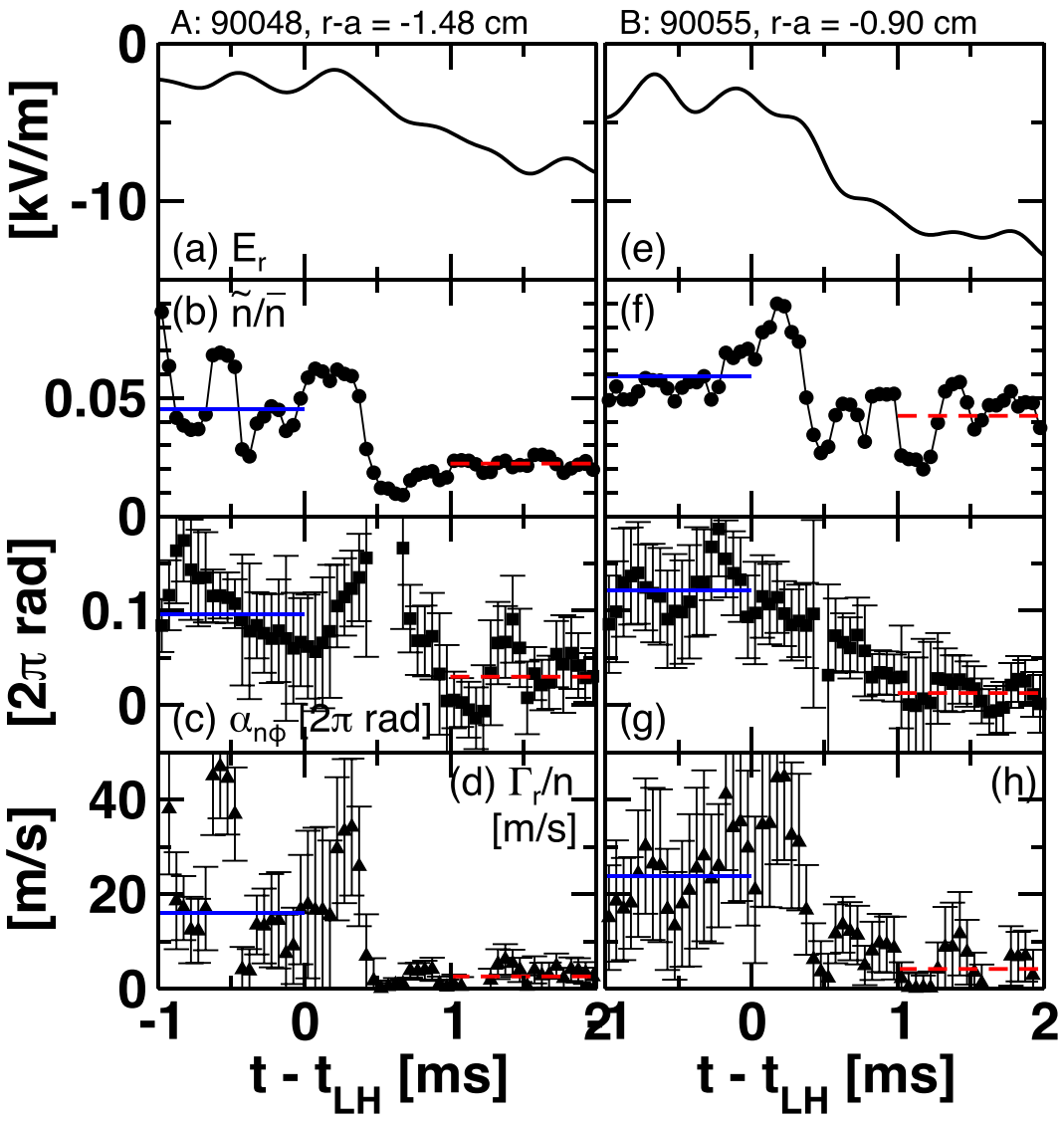

Figure 4. Time traces of (**a**) radial electric field E_r, (**b**) relative density fluctuation amplitude, (**c**) cross phase between density fluctuation and potential fluctuation, and (**d**) particle flux at $r - a = -1.48$ cm. (**e**–**h**) Those at $r - a = -0.90$ cm. Blue-solid and red-dashed horizontal lines in (**b**–**d**) and (**f**–**h**) are mean values in L-mode and MH-mode, respectively.

transition can be described by an integrated system of physics, which is referred to as "single-step" transition in Ref.[31]. In the preset case, however, the turbulence driven radial electric field accounts for only a small fraction of the total one[28] (referred to as "two-step" transition[31]).

Comparing the $\tilde{n}/\bar{n}$ profiles in L-mode and MH-mode, Z_1 seems to be more effective for reducing turbulence amplitude than Z_2. Note that around the radius of the Z_2 peak, the density pedestal appears in which linear energy input to the turbulence is enhanced. The $\tilde{\phi}$ profile has a pivot point at $r - a \sim -0.4$ cm, inside or outside which the turbulence amplitude decreases or increases, respectively. A sign dependence of E_r shear for $\tilde{\phi}$ suppression possibly exists as discussed in Ref.[19]. A mild reduction in $\gamma^2_{n\phi}$ is also seen. Cross phase $\alpha_{n\phi}$ approaches zero in $-3\text{cm} \leq r - a \leq -0.3\text{cm}$, while outside the region $\alpha_{n\phi}$ becomes negative. Non-adiabatic response of electrons on potential perturbation that gives birth to the outward particle flux is weakened. Figure 3(h) shows profile of the particle flux normalized by mean density. The value in L-mode is in a similar order to that reported in Ref.[32] in which the turbulence particle flux is identified as the dominant loss channel of plasma density. As a result of changes mainly in the density fluctuation amplitude and the cross phase, the particle flux is drastically reduced.

Detailed time evolution during the transition is shown in Fig. 4. Left and right columns are time traces for $r - a \sim -1.48$ cm (#90048) and for $r - a \sim -0.90$ cm (#90055), respectively, in which either Z_1 or Z_2 predominantly varies. Time scale of change in E_r non-uniformity is considered to be equivalent as that in E_r. For both cases, time scale of the E_r transition is the order of 100 μs. After the transition, a slow draft of E_r further deepens the transport barrier in the MH-mode state. The relative density fluctuation amplitude immediately responds to change in E_r with the time scale of the order of 100 μs. The change in the amplitude saturates prior to E_r.

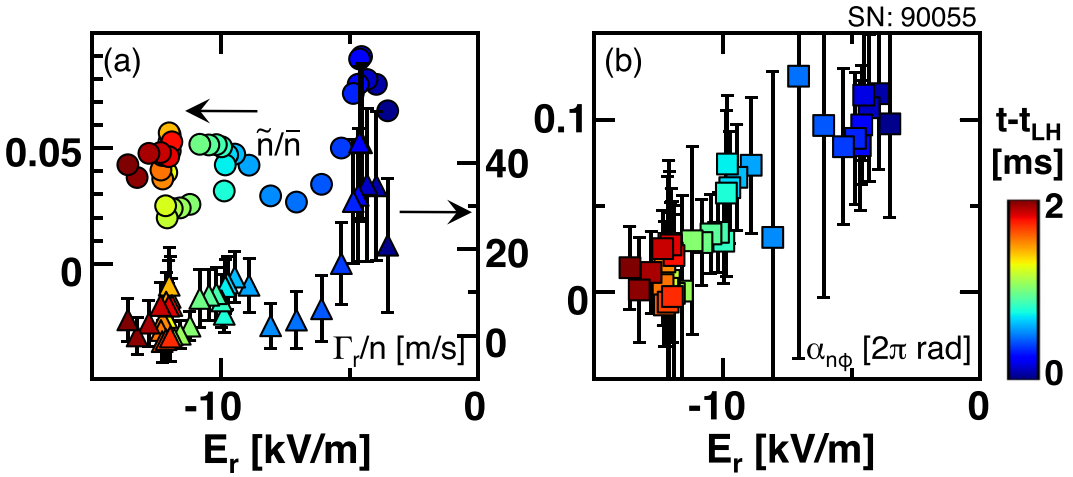

Figure 5. (**a**) Relative density fluctuation amplitude and particle flux and (**b**) cross phase plotted as a function of radial electric field E_r. Color of symbols corresponds to time, which is shown by the color bar.

Meanwhile, the change in the cross phase is much slower. The time scale of the change is 500 μs to 1 ms. These tendencies are common for both cases. The difference of time scale may suggest different underlying physics for density fluctuation amplitude suppression and cross phase modification. Note that the potential fluctuation amplitude is less sensitive to the change in the radial electric field in particular at the E_r-well location as shown in Fig. 3. Models taking into account the different responses in density fluctuation and potential fluctuation are highly desirable in future.

For the case of #90055, the relative density fluctuation amplitude, the cross phase, and the particle flux are plotted as a function of E_r in Fig. 5. The relative density fluctuation amplitude decreases as E_r grows when $E_r > -7$ kV/m. Correspondingly, the particle flux decreases, suggesting that the paradigm of turbulence transport suppression through amplitude effectively works when the E_r non-uniformity is relatively small. Throughout the change in E_r the cross phase gradually approaches zero. With larger value of the E_r non-uniformity the change in the cross phase dominates change in the particle flux.

Discussion and summary

Even inside radii where radial electric field non-uniformity are small, turbulence amplitude in both relative density fluctuation and potential fluctuation are reduced, as observed in CCT[18]. One of the possible mechanisms that can bring this disparate space turbulence suppression is "*turbulence spreading*"[33]. Dynamic inward transmission of a turbulence packet was observed in a limit cycle oscillation event[26]. This observation can provide a clue to address a long-standing mystery, that is, the fast improvement of core confinement by edge transport barrier[34].

In conclusion, we investigated response of turbulent particle flux on radial electric field shear and curvature measured by heavy ion beam probe. Particle flux was mainly suppressed by reducing density fluctuation amplitude and cross phase between density fluctuation and potential fluctuation. Both radial electric field shear and curvature were responsible for transport suppression. Turbulence amplitude reduction immediately responded to the growth of the radial electric field non-uniformity and saturates, while cross phase continuously approached zero.

Methods

JFT-2M. The experiments were conducted in the JFT-2M tokamak, which has a major radius of 1.3 m and a minor radius of 0.3 m. Plasma was auxiliary heated by a co-injected neutral beam (NB) with the power of 750 kW, which is just above the L-H transition threshold. Line averaged electron density was $1.1 \times 10^{19}\ m^{-3}$ before the L-H transition. An upper single-null divertor configuration was employed with the ∇B drift of ion directed toward the X-point. Other operation parameters were as follows: toroidal magnetic field at the magnetic axis B_t of 1.17 T, safety factor at the flux surface enclosing 95% of the total poloidal flux, q_{95}, of 2.9, and plasma current I_p of 190 kA.

Heavy Ion Beam Probe (HIBP). In order to diagnose electrostatic potential ϕ, heavy ion beam is injected from the top-side of the torus, which is ionized doubly inside the confined plasma. By analyzing the secondary beam energy, ϕ is given at four sample volumes (6 mm × 2 mm) with a sampling rate of 1 μs[30]. Radial distance between each sample volume projected in the outer mid-plane is ~2.5 mm. With precise tuning of the HIBP measurement conditions, such as the primary beam energy, the toroidal magnetic field, and the incident angle of the beam, measurement positions can be scanned in an edge region (-5 cm $< r - a < 0$ cm) on a shot-to-shot basis. Relative secondary beam current fluctuation $\tilde{I}_{HIBP}/\bar{I}_{HIBP}$ is regarded to be equivalent to relative electron density fluctuation $\tilde{n}/\bar{n}$, since beam attenuation effect is estimated to be negligibly small at the edge[35]. Gradient of quantities is defined by the finite difference of the neighboring sampling volumes.

Turbulence suppression model. In the newly developed theoretical model[12], amplitude of turbulence having a perpendicular wavenumber k is reduced by the shear factor Z_1 and the curvature factor Z_2 as $I/I_0 = [1 + (k\rho_i)^{-2}(Z_1 + Z_2)]^{-1}$, where I and I_0 are the reduced turbulence amplitude and the intrinsic turbulence amplitude without E_r effects, respectively. Shear factor $Z_1 \equiv \rho_i^2(V_dB)^{-2}E_r'^2$ and curvature factor $Z_2 \equiv -\rho_i^2(V_dB)^{-2}(E_r - V_{tor}B_\theta)E_r''$ are defined as indicators of significance of shear decorrelation and of modulational coupling, respectively, where ρ_i is the ion gyro-radius, $V_d \equiv T|n'|/enB$ is the diamagnetic velocity, and prime is the radial derivative. In the present case, $E_r \gg V_{tor}B_\theta$ is considered to hold[7] so that the toroidal velocity correction term for Z_2 is neglected. Recent investigation in JT-60U[8] showed an important role of not only Z_1 but also of Z_2 by referring to temperature gradient profile as an indicator of confinement intensity.

References

1. Hughes, D., Rosner, R. & Weiss, N. *The Solar Tachocline* (Cambridge University Press, 2007).
2. Diamond, P. H., Itoh, S.-I., Itoh, K. & Hahm, T. S. Zonal flows in plasma – a review. *Plasma Phys. Control. Fusion* **47**, R35 (2005).
3. Wagner, F. *et al*. Regime of improved confinement and high beta in neutral-beam-heated divertor discharges of the ASDEX Tokamak. *Phys. Rev. Lett.* **49**, 1408–1412 (1982).
4. Itoh, S.-I. & Itoh, K. Model of L to H-mode transition in tokamak. *Phys. Rev. Lett.* **60**, 2276–2279 (1988).
5. Shaing, K. C. & Crume, E. C. Jr. Bifurcation theory of poloidal rotation in tokamaks: A model for L-H transition. *Phys. Rev. Lett.* **63**, 2369 (1989).
6. Groebner, R. J. *et al*. Role of edge electric field and poloidal rotation in the LH transition. *Phys. Rev. Lett.* **64**, 3015 (1990).
7. Ida, K. *et al*. Edge electric-field profiles of H-mode plasmas in the JFT-2M tokamak. *Phys. Rev. Lett.* **65**, 1364–1367 (1990).
8. Kamiya, K. *et al*. Experimental validation of non-uniformity effect of the radial electric field on the edge transport barrier formation in JT-60U H-mode plasmas. *Sci. Rep.* **6**, 30585 (2016).
9. Staebler, G. M. & Dominguez, R. R. Electric field effects on ion temperature gradient modes in a sheared slab. *Nucl. Fusion* **31**, 1891 (1991).
10. Sidikman, K. L., Carreras, B. A., Diamond, P. H. & Garcia, L. Theory of electric-field curvature effects on long-wavelength drift wave turbulence. *Phys. Plasmas* **1**, 1142–1153 (1994).
11. Carreras, B. A., Lynch, V. E. & Garcia, L. Effect of a poloidal shear flow on the probability of accessing the multiple saturated states in the resistive interchange instability. *Phys. Fluids B* **5**, 1795–1803 (1993).
12. Itoh, K. *et al*. On Width of Pedestal in the H-mode. *Nucl. Fusion* **57**, 022005 (2017).
13. Biglari, H., Diamond, P. H. & Terry, P. W. Influence of sheared poloidal rotation on edge turbulence. *Phys. Fluids B* **2**, 1 (1990).
14. Terry, P. W., Newman, D. E. & Ware, A. S. Suppression of transport cross phase by strongly sheared flow. *Phys. Rev. Lett.* **87**, 185001 (2001).
15. Kim, E.-J. & Diamond, P. H. Effect of mean flow shear on cross phase and transport reconsidered. *Phys. Rev. Lett.* **91**, 075001 (2003).
16. Itoh, K., Itoh, S.-I., Kamiya, K. & Kasuya, N. On the spatial structure of solitary radial electric field at the plasma edge in toroidal confinement devices. *Plasma Phys. Control. Fusion* **57**, 075008 (2015).
17. Ritz, C. P., Lin, H., Rhodes, T. & Wootton, A. Evidence for confinement improvement by velocity-shear suppression of edge turbulence. *Phys. Rev. Lett.* **65**, 2543 (1990).
18. Tynan, G. *et al*. Steady-state convection and fluctuation-driven particle transport in the H-mode transition. *Phys. Rev. Lett.* **68**, 3032 (1992).
19. Moyer, R. A. *et al*. Beyond paradigm: Turbulence, transport, and the origin of the radial electric field in low to high confinement mode transitions in the DIII-D tokamak. *Phys. Plasmas* **2**, 2397–2407 (1995).
20. Shats, M. *et al*. Inward turbulent transport produced by positively sheared radial electric field in stellarators. *Phys. Rev. Lett.* **84**, 6042 (2000).
21. Antoni, V. *et al*. Electrostatic transport reduction induced by flow shear modification in a reversed field pinch plasma. *Plasma Phys. Control. Fusion* **42**, 83 (2000).
22. Boedo, J. A. *et al*. Scaling of plasma turbulence suppression with velocity shear. *Nucl. Fusion* **42**, 117 (2002).
23. Manz, P. *et al*. Zonal flow triggers the lh transition in the experimental advanced superconducting tokamak. *Phys. Plasmas* **19**, 072311 (2012).
24. Shesterikov, I. *et al*. Experimental Evidence for the Intimate Interaction among Sheared Flows, Eddy Structures, Reynolds Stress, and Zonal Flows across a Transition to Improved Confinemen. *Phys. Rev. Lett.* **111**, 055006 (2013).
25. Yan, Z. *et al*. Observation of the l- h confinement bifurcation triggered by a turbulence-driven shear flow in a tokamak plasma. *Phys. Rev. Lett.* **112**, 125002 (2014).
26. Kobayashi, T. *et al*. Spatiotemporal Structures of Edge Limit-Cycle Oscillation before L-to-H Transition in the JFT-2M Tokamak. *Phys. Rev. Lett.* **111**, 035002 (2013).
27. Ido, T. *et al*. Observation of the Fast Potential Change at L-H Transition by a Heavy-Ion-Beam Probe on JFT-2M. *Phys. Rev. Lett.* **88**, 055006 (2002).
28. Kobayashi, T. *et al*. Experimental Identification of Electric Field Excitation Mechanisms in a Structural Transition of Tokamak Plasmas. *Sci. Rep.* **6**, 30720 (2016).
29. Powers, E. J. Spectral techniques for experimental investigation of plasma diffusion due to polychromatic fluctuations. *Nucl. Fusion* **14**, 749 (1974).
30. Ido, T. *et al*. Observation of the interaction between the geodesic acoustic mode and ambient fluctuation in the JFT-2M tokamak. *Nucl. Fusion* **46**, 512 (2006).
31. Terry, P. W. Suppression of turbulence and transport by sheared flow. *Rev. Mod. Phys.* **72**, 109 (2000).
32. Wootton, A. J. *et al*. Fluctuations and anomalous transport in tokamaks. *Phys. Fluids B* **2**, 2879 (1990).
33. Hahm, T. S. *et al*. Turbulence spreading into the linearly stable zone and transport scaling. *Plasma Phys. Control. Fusion* **46**, A323 (2004).
34. Cordey, J. G. *et al*. A numerical simulation of the LH transition in JET with local and global models of anomalous transport. *Nucl. Fusion* **35**, 101 (1995).
35. Ross, D. W. *et al*. Effect of beam-attenuation modulation on fluctuation measurements by heavy-ion beam probe. *Rev. Sci. Instrum.* **63**, 2232–2240 (1992).

Acknowledgements

We thank professors P. H. Diamond, G. R. Tynan, U. Stroth, J.-Q. Dong, K. J. Zhao, C. Hidalgo, K. Hoshino, M. Sasaki and Y. Kosuga for useful discussions, and the late H. Maeda, Y. Hamada, M. Mori, Y. Kamada, and S. Sakakibara for strong support. This work is partly supported by the Grant-in-Aid for Scientific Research of JSPS, Japan (17K14898, 15H02155, 16H02442), the collaboration programs of JAEA and of the RIAM of Kyushu University and Asada Science Foundation.

Author Contributions

T.I., K.K., and Y.M. conducted the experiments. T.I. provided the HIBP data. T.K. analyzed the data. K. Itoh and SII provided the theoretical models. T.K., K. Itoh, T.I., K.K., S.I.I., Y.N., A.F., S.I. and K. Ida discussed the model validation. T.K. and K. Itoh wrote the main manuscript text and all authors reviewed the manuscript.

Additional Information

Competing Interests: The authors declare that they have no competing interests.

Publisher's note: Springer Nature remains neutral with regard to jurisdictional claims in published maps and institutional affiliations.